Mission-driven path planning and design of submersible unmanned ship with multiple navigation states

Jia Guo[1], Yuanhang Hou[1, 2#], Xiao Liang[1], Hongyu Yang[1], Yeping Xiong[2]
1. Naval Architecture and Ocean Engineering College, Dalian Maritime University, Dalian 116026, China
2. Faculty of Engineering and Physical Sciences, University of Southampton, Boldrewood Innovation Campus, SO16 7QF Southampton, UK
Corresponding author: Yuanhang Hou
Email: houyuanhang@dlmu.edu.cn

Abstract: The path planning of unmanned ships at the lowest energy consumption is of great significance for energy savings. At present, the path planning of unmanned ships based on the idea of energy savings is usually oriented toward a single navigation state, and there are few research projects on the path planning of ships that sail across multiple navigation states. The navigation states of submersible unmanned ships of path planning in this paper involves underwater navigation states with various diving depths and water's surface navigation state. The improved genetic algorithm is applied to carry out the path planning for a single navigation state and task-driven multi-navigation states of the submersible unmanned ship at energy-saving velocity and non-energy-saving velocity, respectively. The energy-saving velocities are obtained by establishing optimization models. The results show that, at energy-saving velocity, the energy consumption of the same type of navigation paths increase with the diving depth. There is an obvious velocity demarcation point at non-energy-saving velocity range, which makes the sequence of energy consumption of the three types of paths classed by navigation tasks reversed before and after that point. The research can provide technical support for path planning of cross-domain unmanned ships.

Key words: submersible unmanned ship, path planning, multi-navigation state, navigation state transition, improved genetic algorithm, energy consumption

1 Introduction

As a new-concept, unmanned platform with cross-domain navigation capability, the submersible unmanned ship can convert the surface and underwater navigation states by adjusting parameters such as displacement and velocity. It has unique advantages in military, scientific research and civilian fields due to its excellent positioning ability, long endurance and excellent navigation performance. In order to better develop marine resources, accelerate the utilization and protection of marine resources. As well as to provide better safety guarantee for submersible unmanned ships navigating and working in complex and changeable marine environment, path planning is a marine technology that should be vigorously developed.

The United Kingdom, the United States have already applied them to the military field, and other countries are in the beginning stages of research on multi-state ships. The OceanAero Corporation of the United States has developed the Submaran multi-state small unmanned aerial vehicle [2]. The semi-submersible gas turbine of the SSGT multi-vehicle, launched by the British BMT company, provides power, and the fuel cell provides power during concealed sailing [2]. The French company DCNS has launched the SMX-25 multi-navigation concept submarine [3]. British BMT company has developed an all-electric multi-state submarine - SSGT submarine [3]. Similar studies in China are mostly theoretical studies or model tests. Huo Cong et al. [4] verified the feasibility of the continuous transformation of the flight state by conducting self-propelled model tests and numerical simulations of a latent high-velocity ship. Wang Wei [2] analysed the change process of the navigation state of a certain multi-navigation-state

ship through a numerical simulation and tank-towing test and verified that navigation state conversion can only be realised under specific trim angle and velocity conditions. Luo Fuqiang et al. [5] conducted a hydrostatic model towing test of the multi-navigation high-velocity unmanned boat from the semi-submersible state to the surface state and verified that it has good resistance performance and motion attitude within a certain draft range. The above research on multi-navigation-state ships verifies the feasibility of navigation state changes and has great reference significance for the subsequent design and research of submersible unmanned ships.

In recent years, research on path planning for underwater robots has emerged in an endless stream. Zeyad Abd Algfoor [6] et al. proposed a new path planning method based on the A* algorithm, the bidirectional A* algorithm and the jump point pathfinding method, which reduced the search time of the heuristic algorithm. Eichhorn et al. [7] proposed several important practice-oriented requirements for the optimal path planning for the AUV "SLOCUM Glider" and a solution based on fast graph algorithm. Yu et al. [8] proposed a fast travel method for AUV path planning in a 3D large-scale battlefield environment, which solved the problems of high AUV discovery probability, safe navigation and low fuel consumption. Gore et al.[9] proposed an efficient algorithm for dynamically estimating the target path and re-planning the shortest path from the AUV to the target faster. Pan et al. [10] proposed a genetic-ant hybrid algorithm to solve the problems of low efficiency and long search time in path planning in the three-dimensional space environment, and the designed partitioning method reduced the population search range. Li et al. [11] proposed a vortex time-domain quantum artificial bee colony optimization algorithm for the distributed task planning model of multi-autonomous underwater robots to solve the optimal task planning scheme for multi-AUV. Ramos et al. [12] planned a path to optimise scientific returns and navigation efficiency using the complex spatiotemporal structure of the ocean current field and demonstrated the ability of dynamical system theory to achieve this goal by implementing the Silbo trans-North Atlantic AUV real-time navigation strategy. Lin et al. [13] integrated the dynamic routing algorithm based on particle swarm optimisation, a self-tuning fuzzy controller, stereo vision detection technology and a 6-DOF mathematical model into the autonomous underwater vehicle detection system, which more effectively realised dynamic path planning. Mahmoudzadeh et al. [14] proposed a hybrid path planning model for the task assignment and management of underwater robots after considering the constraints of mission time, battery, and potential operating field uncertainty and variability, providing efficient performance. Reference [15] developed an advanced reactive mission planner for AUVs in uncertain underwater environments. According to the assignment of mission priorities, the AUVs were guided towards the target of interest and managed to complete the mission on time. Sun Yushan et al. [16] adopted the deep reinforcement learning method to realizse global path planning for an AUV in a large-scale 3D environment. Hassan Sayyaadi et al. [17] applied the proposed stochastic real-value augmented learning algorithm to the path planning research on AUVs, which improved the adaptability of AUVs to the ocean. In [18], a GBNN algorithm based on discrete and centralised programming is proposed, which enables the underwater robot to plan a reasonably collision-free coverage path and achieve full coverage in the same task area as in the case of division of labor and cooperation. Reference [19] proposes an AUV path optimization algorithm based on energy consumption optimization and improved ant colony algorithm. The purpose of energy consumption guiding ant colony evolution is realized. The algorithm has certain advantages in reducing the energy consumption of underwater robots and improving the endurance. Alvarez et al. [20] minimizes the energy cost by changing the propulsion speed of the AUV to keep the speed of the AUV relative to the seabed constant, and finally find a safe path to take the vehicle from the starting position to the mission-specified destination. Witt et al. [21] describes a new optimal path planning strategy, the described solution utilizes ocean currents to achieve mission objectives with minimal energy consumption, or trade-offs between mission time and required energy. The proposed algorithm uses parallel group search as a means to reduce the apparent sensitivity of the complex cost to large local minima.

The above research proves the innovativeness, effectiveness and superiority of considering multiple factors and updating the optimisation algorithm in path planning, which has great reference significance for path planning design and research for surface ships, underwater vehicles and submersible unmanned ships. However, unlike surface or underwater vehicles, the submersible unmanned ship has surface navigation, semi-submersible and underwater diving capabilities and can perform cross-domain navigation. In other words, it can realise the transformation between navigation states. Therefore, it is of great significance to

explore the relevant laws of the navigation path of the submersible unmanned ship after determining the navigation target. Considering the concept of energy-saving navigation, the mission-driven path planning of the submersible unmanned ship is designed and studied. After classifying the navigation tasks, the research process and scheme of the path planning are further refined and improved. The influence of velocity and diving depth on the navigation path is emphasized, and the hydrostatic resistance test of different diving depths before the path planning simulation greatly improves the accuracy of the conclusions of the manuscript. At the same time, several improvements have been made to the genetic algorithm used in path simulation. The improved algorithm has certain advantages in reducing path energy consumption. The comparison before and after the algorithm improvement will be described in Chapter 5 of the manuscript.

2 Description of the research problem

Energy consumption is a key factor to be considered in the process of exploring path planning for submersible unmanned ships. In order to achieve energy savings, it is necessary to investigate the performance of submersible unmanned ships at different diving depths. In this paper, two models, the energy consumption-based velocity optimisation model and the navigation path energy consumption model, are established. The model information comes from the resistance performance test performed by submersible unmanned ship.

Path planning is divided into energy-saving speed path planning and non-energy-saving speed path planning, which are carried out in two-dimensional navigation space and three-dimensional navigation space respectively. When the diving unmanned ship encounters obstacles in the two-dimensional navigation space, it adopts the obstacle avoidance method of turning around the obstacles on the water surface. When encountering obstacles in the three-dimensional navigation space, the obstacle avoidance method combines the two methods of avoiding obstacles by turning around on the water surface and diving under the obstacles and then floating up to the water surface to avoid obstacles.

At the same time, navigation tasks are set under the obstacles in the three-dimensional navigation space. The paths in the three-dimensional navigation space are subdivided into three categories according to the different floating positions of the submersible unmanned ship after completing the underwater task. Finally, the energy consumption comparison of various navigation paths of the submersible unmanned ship in different navigation space dimensions is explored.

3 Methodology

3.1 Resistance performance test

In order to determine the navigation resistance of the submersible unmanned ship at different diving depths, a resistance performance test of the submersible unmanned ship was carried out before the path planning, and the total length of the test model was designed to be 1.6m. More detailed test ship model descriptions are shown in the table 1 below. The underwater resistance sensor used was calibrated before the test, and it was found that the linear relationship between the load and the output was good and the accuracy met the requirements.

Table 1. Parameters of the test ship model

Ship form parameters	value
Length (m)	1.6452
L_{BP} (m)	1.6000
Beam (m)	0.2322
Depth (m)	0.1408
Draft (m)	0.0868
Wetted surface (m^2)	0.4451

Hydrostatic resistance at velocitys of 0.4m/s, 0.6m/s, 0.8m/s, 1.0m/s, 1.1m/s, 1.2m/s, 1.3m/s, 1.4m/s, 1.5m/s, 1.6m/s and

1.7m/s were tested for each diving depth. The diving depths corresponding to working conditions 0# to 4# are 0m, 0.32m, 0.48m, 0.64m and 0.96m, respectively. The definition of diving depth is shown in Figure 1.

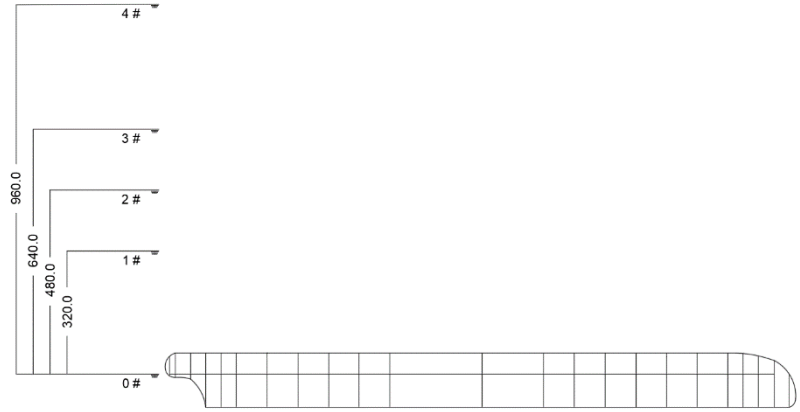

Figure 1. Definition of diving depth

The 0# condition (dive depth 0m) is the surface navigation condition, and the diving unmanned ship is located between water and air, that is, it is not completely submerged in water. Working conditions 1#~4# (diving depths of 0.32m, 0.48m, 0.64m, 0.96m) are underwater working conditions. Under these four working conditions, the submersible-floating unmanned ship is completely immersed in water. The test data are shown in Table 2.

Table 2. Resistance data

Velocity(m/s)	F_z(N)|(0m)	F_{z1}(N)|(0.32m)	F_{z2}(N)|(0.48m)	F_{z3}(N)|(0.64m)	F_{z4}(N)|(0.96m)
0.4	29.3	39.6	37.3	28.7	33.9
0.6	54.6	73.7	72.6	63	71.6
0.8	85.8	124.5	127.0	117.2	124.1
1.0	124.9	198.4	193.1	182.6	190.8
1.1	150.2	226.3	232.9	227.7	227.9
1.2	181.4	272.1	274.7	267.5	273.1
1.3	214.6	327.0	321.1	312.9	323.1
1.4	277.0	393.5	377.9	361.1	367.4
1.5	398.0	481.7	439.1	421.4	414.0
1.6	581.4	594.6	509.8	480.5	474.8
1.7	776.5	709.5	593.1	548.0	533.0

Resistance data is fitted with the polyfit function in Matlab, and the relationship between velocity and resistance is obtained, as shown in Equation (3). The fitting result is shown in Figure 2.

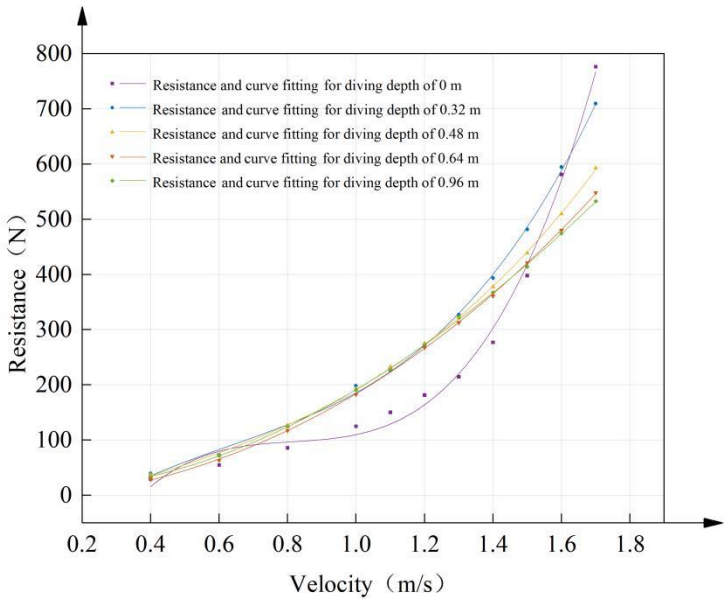

Figure 2. Resistance curve fitting

$$\begin{cases} F_z = 916.51V_w^3 - 2239.2V_w^2 + 1861.8V_w - 429.44 \\ F_{z1} = 319.4691V_{u1}^3 - 608.1841V_{u1}^2 + 604.1032V_{u1} - 129.7356 \\ F_{z2} = 100.7287V_{u2}^3 - 73.8915V_{u2}^2 + 206.5016V_{u2} - 42.0903 \\ F_{z3} = 19.966V_{u3}^3 + 135.93V_{u3}^2 + 39.387V_{u3} - 11.377 \\ F_{z4} = -14.1726V_{u4}^3 + 216.6493V_{u4}^2 - 18.9138V_{u4} + 7.7503 \end{cases} \quad (1)$$

where F_z, F_{z1}, F_{z2}, F_{z3} and F_{z4} are the navigation resistance of the unmanned ship for various diving depth corresponding to working conditions 0# to 4#, V_w, V_{u1}, V_{u2}, V_{u3} and V_{u4} are the sailing velocity for various diving depth corresponding to working conditions 0# to 4#.

3.2 Brief analysis of energy consumption

The energy consumption of the submersible unmanned ship is mainly due to the power propulsion module and the electrical equipment module. The energy consumption of power equipment mainly refers to the energy consumption of the propulsion system, namely the propeller. The energy consumption of electrical equipment includes the energy consumption of electronic equipment, such as navigation systems, communication systems and control systems [22]. In general, the power consumption of such equipment is determined. The amount of energy consumption also depends on the working time of each module in the submersible unmanned ship, which is approximated by the sailing time of the complete voyage. The energy consumption of the complete path of the submersible unmanned ship, from the starting point to the target point, can be expressed by equation (2).

$$E = (P_e + P_p) * T \quad (2)$$

where P_e is the power of the electrical equipment, P_p is the power of the power equipment and T is the total navigation time for continuous path.

3.3 Improved genetic algorithm – Navigation path optimisation

The method applied in the path simulation for the submersible unmanned ship in the following is an improved genetic algorithm that has three steps: selection, crossover and mutation.

3.3.1 Select operation

The selection operation adopts the roulette method, and the basis of this method is that the probability of each individual being

selected is proportional to its fitness. In order to effectively improve the convergence velocity of the algorithm, an elite selection strategy is added to the traditional genetic algorithm, and the individual with the highest fitness value in the contemporary population is selected to be directly retained in the next generation and does not participate in subsequent operations, such as selection, crossover, and mutation in the genetic algorithm. The fitness of individuals retained by the elite selection strategy is shown in formula (3):

$$f(a_k(t)) = \max\left\{ f(a_1(t)), f(a_2(t)), \ldots, f(a_k(t)) \right\} \tag{3}$$

After the elite selection strategy is completed, the retained individual $a_k(t)$ must be compared with the optimal individual $a_k(t+1)$ of the next generation. If the fitness value $f(a_k(t))$ of the individual $a_k(t)$ of the previous generation is greater than the fitness value $f(a_k(t+1))$ of the individual $a_k(t+1)$ of the next generation, this means that the population has not evolved, and the elite individual will replace the individual with the worst fitness value in the next generation, effectively preventing the worst individual from participating in the genetic operation. The process of obtaining the optimal and worst fitness values of the next generation individuals is shown in equations (4) and (5):

$$f_{\max}(a_k(t+1)) = \max\left\{ f(a_1(t+1)), f(a_2(t+1)), \ldots f(a_k(t+1)) \right\} \tag{4}$$

$$f_{\min}(a_k(t+1)) = \min\left\{ f(a_1(t+1)), f(a_2(t+1)), \ldots f(a_k(t+1)) \right\} \tag{5}$$

3.3.2 Cosine adaptive crossover and mutation operations

The intersectional operation in the path planning adopts the single-point intersection method, and the intersection point is that of the two intersecting parent paths, except for the starting point and the target point. The two parent paths before the intersection remain unchanged, and the two parent paths after the intersection are interchanged. After intersection, two new child paths are formed.

The mutation operation adopts the two-point mutation method. In a parent path, two adjacent points, not including the starting point and the target point, are randomly selected, and the original path between the two points is mutated into a new path that is different from the parent path and has the shortest distance.

The determined crossover probability p_c and mutation probability p_m selected in the traditional genetic algorithm directly affect the optimization ability of the genetic algorithm. Therefore, the crossover probability p_c and the mutation probability p_m cannot be selected arbitrarily. In order to improve the convergence velocity and performance of the genetic algorithm, a cosine-type adaptive adjustment function is introduced, which adaptively adjusts the parameters according to the evolution information. Adaptive crossover probability p'_c and adaptive mutation probability p'_m replace p_c and p_m. The adaptive crossover and mutation probabilities are shown in equations (6) and (7).

$$P_c = \begin{cases} \dfrac{p_{c1}+p_{c2}}{2} + \dfrac{(p_{c2}-p_{c1})}{2} * \cos\left(\dfrac{f_{\max}-f'}{f_{\max}-f_{avg}} \cdot \pi \right) & f' \geqslant f_{avg} \\ P_{c2} & f' < f_{avg} \end{cases} \tag{6}$$

where P_{c1} is the initial maximum crossover probability, P_{c2} is the initial minimum crossover probability, f_{max} is the largest fitness value in the population, f_{avg} is the average fitness value of the population and f' is the one with the larger fitness value between two individuals to be crossed.

$$P_m = \begin{cases} \dfrac{p_{m1}+p_{m2}}{2} + \dfrac{(p_{m2}-p_{m1})}{2} * \cos\left(\dfrac{f_{\max}-f}{f_{\max}-f_{avg}} \cdot \pi \right) & f \geqslant f_{avg} \\ P_{m2} & f < f_{avg} \end{cases} \tag{7}$$

where P_{m1} is the initial maximum mutation probability, P_{m2} is the initial minimum mutation probability, f_{max} is the largest

fitness value in the population, f_{avg} is the average fitness value of the population and f is the fitness value for the individual to be mutated.

The variation trand of adaptive crossover and mutation probability with individual fitness value is shown in Figures 3.

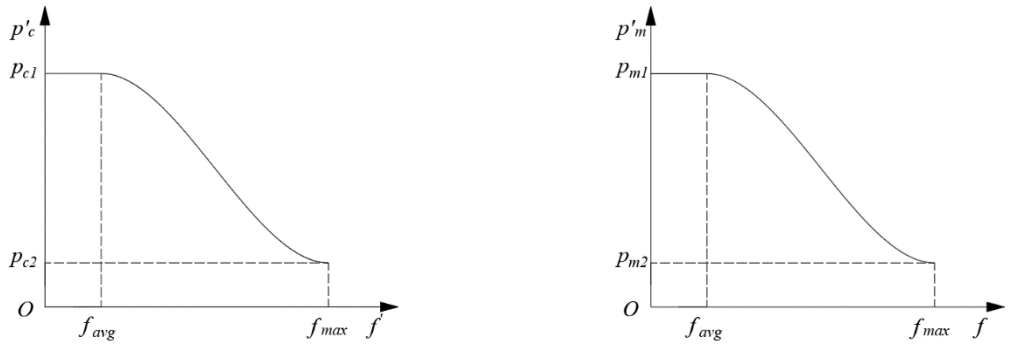

(a)Adaptive crossover probability (b) Adaptive mutation probability

Figure 3. Adaptive crossover and mutation probabilities

When the crossover individual fitness f' is close to the average fitness f_{avg} , the adaptive crossover probability p'_c is relatively large, and the change trend of the curve is relatively slow, which is conducive to the iterative evolution of the population. When the cross-individual fitness f' is close to the population's maximum fitness f_{max} , p'_c is small, and the curve changes smoothly and slowly, which increases the possibility of retaining excellent individuals. The adaptive regulation of mutant individuals is the same as that of crossover individuals.

In this section, the resistance fitting formula for various diving depths obtained from the test is used to establish the velocity-optimisation model under different working conditions. The optimised velocity will be applied to the energy-saving velocity path optimisation part of the submersible unmanned ship.

4.1 Relationship between energy consumption and velocity

Different diving depths (working conditions) have different relationship models between energy consumption and velocity. The five working conditions in this paper are divided into two categories: water's surface working condition and underwater working conditions. Selecting the surface working condition and any underwater working condition to describe the model establishment process in detail, taking working condition 0# (diving depth of 0m) and underwater working condition 2# (diving depth of 0.48m) as examples.

The sailing time is expressed by the length of sailing path and velocity. The sailing time for submersible unmanned ship in working condition 0# is shown in Equation (8).

$$T_w = \frac{D_w}{V_w} \tag{8}$$

The sailing time in condition 2# is shown in Equation (9).

$$T_{u2} = \frac{D_{u2}}{V_{u2}} \tag{9}$$

Since the navigation resistance and the thrust generated by the propeller are equal when the submersible unmanned ship sails at a constant speed, the effective power of the propulsion system can be expressed as Equation (10).

$$P_p = F * V \tag{10}$$

where V is the velocity of submersible unmanned ship and F is the sailing resistance.

Replace F in Equation (10) with the resistance formula for working condition 0# and 2#， the propulsion system powers P_{pw} and P_{pu2} for working conditions 0# and 2# are obtained, respectively.

$$P_{pw} = (916.51V_w^3 - 2239.2V_w^2 + 1861.8V_w - 429.44) * V_w \tag{11}$$

where V_w is the velocity for working condition 0#.

$$P_{pu2} = (100.7287V_{u2}^3 - 73.8915V_{u2}^2 + 206.5016V_{u2} - 42.0903) * V_{u2} \tag{12}$$

where V_{u2} is the velocity for working condition 2#.

Then, the sailing time and propulsion system power of the above two working conditions are respectively substituted into the energy consumption formula (2), and the relationship model between energy consumption and velocity under the two working conditions is obtained:

$$E_w = (916.51V_w^3 - 2239.2V_w^2 + 1861.8V_w - 429.44 + \frac{P_e}{V_w}) * D_w \tag{13}$$

$$E_{u2} = (100.7287V_{u2}^3 - 73.8915V_{u2}^2 + 206.5016V_{u2} - 42.0903 + \frac{P_e}{V_{u2}}) * D_{u2} \tag{14}$$

In the relationship model between energy consumption and velocity, each model corresponds to the energy consumption during sailing under the current working conditions. P_e is the power of electrical equipment, which is a fixed value of 0.8 and has a small impact on the energy consumption of submersible unmanned ships. D_w and D_{u2} are the navigation path lengths.

4.2 Establishment of velocity optimisation model

Energy consumption is affected by velocity and sailing resistance. Considering energy savings, it is not advisable to select an excessively high velocity. Therefore, given the premise of ensuring the safe navigation of the submersible unmanned ship, the velocity of the submersible unmanned ship should be optimised to determine an energy-saving velocity that minimises the energy consumption of navigation.

The design velocity of the submersible unmanned ship used in the test is 2m/s, and the velocity does not exceed this value during the sailing process. The resistance value and energy consumption value under each working condition are all greater than zero.

The minimums value of energy consumption in the surface condition and underwater condition are expressed by Equations (15) and (16):

$$\min E_w = E_p + E_e = (F_w + \frac{P_e}{V_w}) * D_w \tag{15}$$

$$\min E_{un} = E_p + E_e = (F_{un} + \frac{P_e}{V_{un}}) * D_{un} \tag{16}$$

Taking water's surface condition 0# and underwater condition 2# as examples, the velocity optimization models based on energy consumption are established, respectively.

(1) Velocity optimization model of water's surface condition 0#

$$\min E_w = (916.51V_w^3 - 2239.2V_w^2 + 1861.8V_w - 429.44 + \frac{P_e}{V_w}) * D_w \tag{17}$$

$$s.t. \begin{cases} 0 < V_w < V_{MD} \\ 916.51V_w^3 - 2239.2V_w^2 + 1861.8V_w - 429.44 > 0 \\ E_w > 0 \end{cases}$$

(2) Velocity optimization model of water surface condition 2#

$$\min E_{u2} = (100.7287V_{u2}^3 - 73.8915V_{u2}^2 + 206.5016V_{u2} - 42.0903 + \frac{P_e}{V_{u2}}) * D_{u2} \tag{18}$$

$$s.t. \begin{cases} 0 < V_{u2} < V_{MD} \\ 100.7287V_{u2}^3 - 73.8915V_{u2}^2 + 206.5016V_{u2} - 42.0903 > 0 \\ E_{u2} > 0 \end{cases}$$

The velocity optimisation model of all working conditions is established, and the method and process are the same as the above-mentioned working conditions 0# and 2#. After the models are built, the genetic algorithm toolbox in Matlab is called, and

the objective function and constraints are input to optimise energy-saving velocity. Finally, the energy-saving velocity V_{wopt1} of working condition 0# is 0.372m/s. The energy-saving velocities V_{uopt1}, V_{uopt2}, V_{uopt3} and V_{uopt4} for the underwater submersible conditions 1# to 4# are 0.28m/s, 0.22m/s, 0.18m/s and 0.14m/s, respectively. V_{MD} is the design velocity of the submersible unmanned ship.78

5. Path planning simulation for submersible unmanned ship

5.1 Modeling the navigation environment

(1) Create a grid map

In order to visually represent the navigation area of the submersible unmanned ship and the final path of obstacle avoidance, a grid map composed of several unit grids is set up during the simulated navigation of the submersible unmanned ship. Raster maps include surface grid maps and underwater grid maps. On the surface grid map, black represents obstacles, and white represents free-navigation areas. When the submersible unmanned ship sails in the three-dimensional navigation space, in order to avoid obstacles, it will dive to the area completely below the obstacles, so the underwater grid map is set as an all-white freely navigable grid area.

(2) Species code

A Cartesian coordinate system is established, and each grid can be represented by coordinates and serial number points.

(3) Population initialisation

The purpose of population initialisation is to generate multiple feasible paths for the submersible unmanned ship. The path is formed by connecting multiple waypoints generated on the grid map, and the waypoints of a path must traverse the continuous rows of the grid map. Taking water navigation as an example, the distance between adjacent grids is expressed as follows:

$$D = \max\left\{abs(x_{i+1} - x_i), abs(y_{i+1} - y_i)\right\} \tag{19}$$

Then, if the distance between adjacent grid points is 1, the path is regarded as continuous. Otherwise, it is regarded as discontinuous, and when discontinuous, the grid insertion operation is performed until adjacent grids are continuous. If the inserted grid is a free grid, the grid number should be updated to connect with the front and rear grid points so as to form an uninterrupted path. If the inserted grid is an obstacle grid, the submersible unmanned ship will avoid obstacles and re-navigate left, right, up and down.

5.2 Mathematical modeling

The main scale of the submersible unmanned ship used in the test is relatively small. In order to ensure that it can finally sail according to the established route, it is often selected under relatively good sea conditions. Although the difference between the hydrostatic test results and the actual wind and wave conditions exists, it is often very small. In reference [23], the correlation analysis of ship speed, wind speed, wave height, air temperature, water temperature, ice concentration and ship energy efficiency is carried out based on Yongsheng's real sailing data. The correlation coefficients of wind speed, wave height, air temperature and water temperature with energy efficiency are all close to and less than 0.5. The correlation coefficients between ship speed and energy efficiency, ice concentration and energy efficiency are 0.835 and 0.680, respectively. Only ship speed and ice concentration are used as factors affecting energy efficiency in modeling. Similarly, this paper regards speed and diving depth as the main influencing factors of navigation energy consumption. Although such research process and results are slightly different from the real situation, they are still credible. The established mathematical model finally does not consider the influence of wind, waves and other factors on the ship.

5.2.1 Assumption

(1) The path optimisation design process regards the submersible unmanned ship as a mass point. COLREGS stipulates that in the event of a situation, the unmanned boat may maintain the original course and may also need to take deceleration or steering measures to avoid it, and deceleration and steering will affect its energy consumption. Due to the short voyage of this simulation,

the acceleration and deceleration processes of the submersible unmanned ship are ignored, and each voyage is regarded as having a constant velocity sailing.

(2) In the actual navigation process, the submersible unmanned ship will inevitably have bow or stern trim. However, in this path planning process, the trim angle of the submersible unmanned ship is ignored, and both surface navigation and underwater navigation at a certain depth are regarded as floating on even keel.

(3) The transition process from the state of water's surface navigation to the state of underwater diving at a certain depth is assumed to be vertical downward diving, and the transition process from the underwater navigation state at a certain depth to the water's surface navigation state is assumed to be vertical upward floating.

(4) It is assumed that the navigation state of the submersible unmanned ship only changes twice when navigating in the three-dimensional navigation space: the water's surface navigation is transformed into underwater navigation with a certain diving depth, and the underwater navigation with a certain diving depth is changed into water's surface navigation. In other words, there is only one downward dive and one upward ascent. This is to reduce the problem of increased sailing time caused by frequent diving and ascending.

5.2.2 Design variables – Navigation path representation

The navigation path of the submersible unmanned ship is represented by waypoints on the grid map, both the surface grid map and the underwater grid map with different diving depths. After the path point coordinates are determined, the path length is increased by means of accumulation. When the sum of the absolute value of the difference between the abscissa coordinates of the i and i+1 path points and the absolute value of the difference between the ordinate coordinates is equal to 1, the path length increases by 1. If the sum of the above absolute values is not 1, the length of the path increases by $\sqrt{2}$.

After the population is initialised, multiple feasible paths will be generated. Taking the water's surface navigation path as an example, the i-th path is represented as $p_{i1}, p_{i2}, p_{i3}, \ldots, p_{ii}$ are the path points passed by the i-th path and the path length can be expressed as follows:

$$D_w = \sum_{i=1}^{w} D_i = \sum_{i=1}^{w} \sqrt{|x_{i+1} - x_i|^2 + |y_{i+1} - y_i|^2} \tag{20}$$

where D_i is the distance between two adjacent path points, x_{i+1} is the abscissa of the i+1th path point, x_i is the abscissa of the i-th path point, y_{i+1} is the ordinate of the i+1th waypoint and y_i is the ordinate of the i-th waypoint.

5.2.3 Objective function

In order to build a low-energy and high-energy-saving path, the influence of energy consumption factors is mainly considered, and the energy consumption is the objective function value of the path planning of the submersible unmanned ship.

$$E(i) = F * D_i \tag{21}$$

On the basis of calculating the path length, the energy consumption of the complete path is still calculated in an accumulative manner.

$$E(i) = E(i) + \Delta E \tag{22}$$

where ΔE is the energy consumption of the navigation path between the i-th waypoint and the i+1th waypoint.

Taking the water surface grid map as an example, the energy consumption between two adjacent waypoints ΔE is as follows:

$$\Delta E = (916.51V_w^3 - 2239.2V_w^2 + 1861.8V_w - 429.44)\Delta D_i + P_e * (\frac{\Delta D_i}{V_w}) \tag{23}$$

where V_w is the velocity of the water surface, ΔD_i is the distance between the i-th waypoint and the i+1th waypoint and ΔD_i is 1 or $\sqrt{2}$.

The path energy consumption of the submersible unmanned ship when navigating in three-dimensional space includes three parts, namely the energy consumption *E1* of the surface navigation path, the energy consumption *E2* of the diving and ascent paths, and the energy consumption *E3* of the underwater path when the diving depth is determined.Therefore, the objective function of

the three-dimensional navigation space is expressed as follows:

$$E(i) = (916.51V_w^3 - 2239.2V_w^2 + 1861.8V_w - 429.44 + \frac{P_e}{V_w}) * \sum \sqrt{|x_{i+1} - x_i|^2 + |y_{i+1} - y_i|^2} + E_2 + [F_{zn}(V_{un}) + \frac{P_e}{V_{un}}] * \sum \sqrt{|x_{i+1'} - x_{i'}|^2 + |y_{i+1'} - y_{i'}|^2} \quad (24)$$

Where $x_{i+1'}$ and $y_{i+1'}$ are the horizontal and vertical coordinates of the i+1th path point of the underwater grid, respectively, $x_{i'}$ and $y_{i'}$ are the horizontal and vertical coordinates of the i-th path point of the underwater grid, respectively, and $F_{zn}(V_{un})$ is the resistance of the submersible unmanned ship at a certain depth underwater.

The path energy consumption of navigation in the two-dimensional navigation space is only the energy consumption of the water surface navigation, so the objective function of two-dimensional navigation space navigation is expressed as follows:

$$E(i) = (916.51V_w^3 - 2239.2V_w^2 + 1861.8V_w - 429.44 + \frac{0.8}{V_w}) * \sum \sqrt{|x_{i+1} - x_i|^2 + |y_{i+1} - y_i|^2} \quad (25)$$

5.3 Path simulation

This part of the path simulation for the submersible unmanned ship includes two parts: energy-saving-velocity path simulation and non-energy-saving-velocity path simulation. Eeach part is carried out in two-dimensional and three-dimensional navigation spaces, respectively. The path planning of 3D navigation space is task driven.

Before using the improved genetic algorithm to simulate the path, in order to verify the optimization effect of the improved algorithm, two groups of working conditions were selected to use the algorithm before and after the improvement to simulate the path and compare the results. Randomly selected path 1 is a surface navigation path using economical speed. Path 2 is a path with a diving depth of 0.48m in the three-dimensional navigation space. The comparison results of the two working conditions are shown in Table 3 and Table 4. The comparison of the results proves the effectiveness of the improved algorithm.

Table 3. Comparison of simulation results before and after improvement (two-dimensional navigation space path)

Algorithm name	Path node/(-)	Path length/(m)	Path energy consumption/(J)	Path time/(s)
Traditional Genetic Algorithm	17	30.97	80.88	83.25
Improved Genetic Algorithm	9	27.23	71.07	73.15
Optimization rate	47%	12.07%	12.12%	12.13%

Table 4. Comparison of simulation results before and after improvement (three-dimensional navigation space path)

Algorithm name	Path node/(-)	Path length/(m)	Path energy consumption/(J)	Path time/(s)
Traditional Genetic Algorithm	18	29.34	76.13	78.60
Improved Genetic Algorithm	10	29.00	71.54	73.87

Optimization rate	44.44%	1.15%	6%	6%

5.3.1 Simulation of energy-saving-velocity path

Energy-saving-velocity path planning means that the velocity of the submersible unmanned ship at different diving depths is the energy-saving velocity of those diving depths, and the energy-saving velocity at different diving depths is obtained from the energy consumption-based velocity optimisation model.

(1) Single-navigation-state path simulation in two-dimensional navigation space

The paths of the two-dimensional navigation space are all water surface paths. The submersible unmanned ship navigates from the starting point to the target point at an energy-saving velocity of 0.372m/s, avoiding obstacles, and the complete path energy consumption is 71.07J. The route diagram and energy consumption iteration diagram of the voyage are shown in Figures 4.

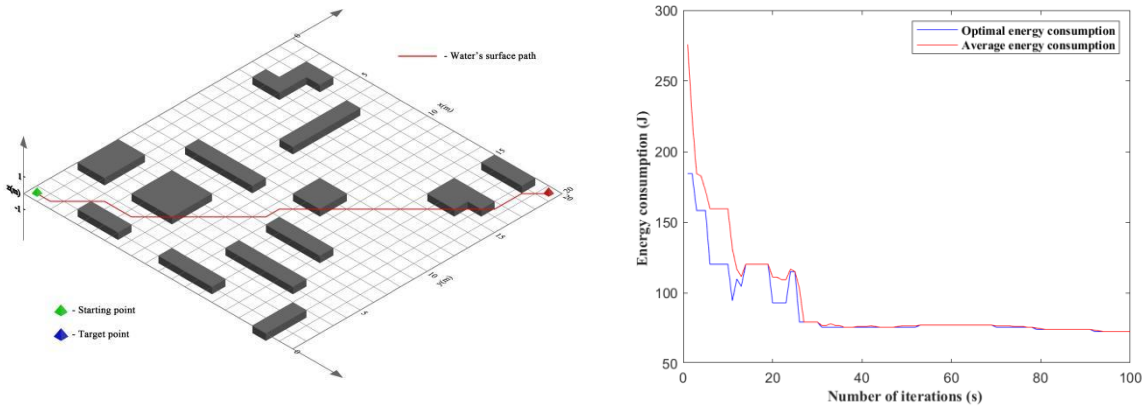

(a) Energy-saving-velocity path (b) Energy consumption iteration diagram

Figure 4. Energy-saving-velocity path planning diagram and energy consumption iterative diagram in two-dimensional navigation space

(2) Multy-navigation-states path simulation in three-dimensional navigation space

The path of the submersible unmanned ship in the three-dimensional navigation space includes the water's surface path, the path of transition between different navigation states and the underwater path. The transition path between different navigation states of each complete path is determined and unique. The above assumes that the transition paths are vertical paths, and the energy consumption of vertical paths at different depths is calculated separately.

It can be seen from the navigation map that three obstacles of different sizes and shapes are located on the line connecting the starting point and the target point of the navigation map. A navigation task exists under the obstacle that is closest to the starting point. The submersible unmanned ship must dive under this area to complete the navigation task. In other words, the area under the obstacle must have a partial navigation path. After completing the navigation task, the paths are divided into three categories according to the ratio of the underwater path length to the total path length or the floating position. Taking the diving depth of 0.48m as an example, the height of the obstacle is less than 0.48m. When other dive depths are determined, the height of the obstacle is less than the diving depth.

After the submersible unmanned ship completes the navigation task and passes through the area under the task obstacle, it immediately rises to the water surface vertically, and the path that continues to sail on the water surface and reach the target point is the first type of navigation path. The complete path diagram of the first type of path and the iterative diagram of the three-part

energy consumption are shown in Figure 5. The energy consumption iterative diagram includes the iterative diagrams of the surface path I, the underwater path and the underwater path II.

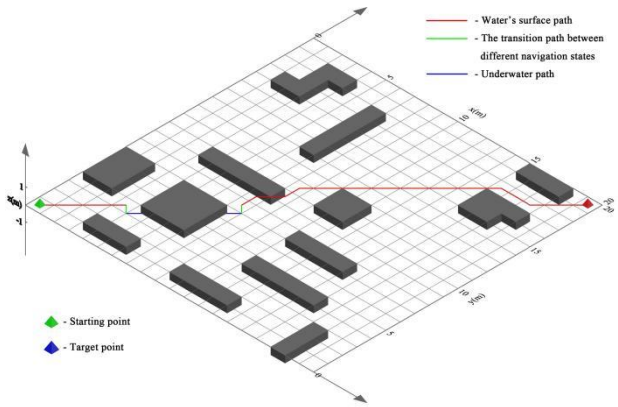

(a) The first type of path with a diving depth of 0.48m

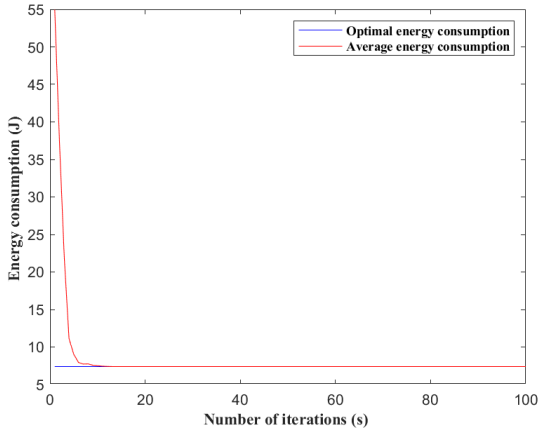

(b) Iterative diagram of water's surface path I

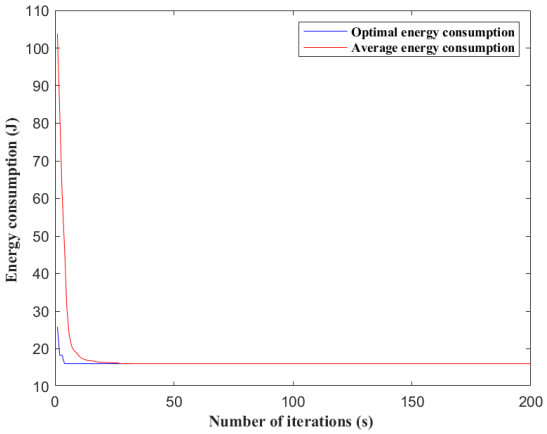

(c) Iteration diagram of underwater path

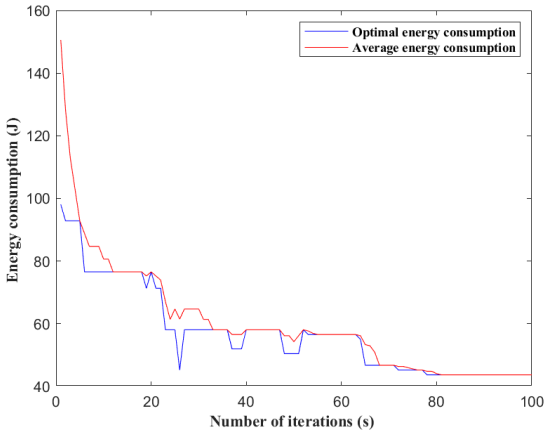

(d) Iterative diagram of water's surface Path Ⅱ

Figure 5. Path planning diagram and energy consumption iterative diagram for the first type of path witin energy-saving-velocity in 3D navigation space (diving depth of 0.48m)

After completing the navigation task, the submersible unmanned ship does not go up to the surface immediately, but, rather, continues to navigate underwater at a certain depth for a period of time, surfaces and continues to navigate on the surface to reach the target point. Such paths are second-class paths.The path graph and iterative graph of the second type of path are shown in Figure 6.

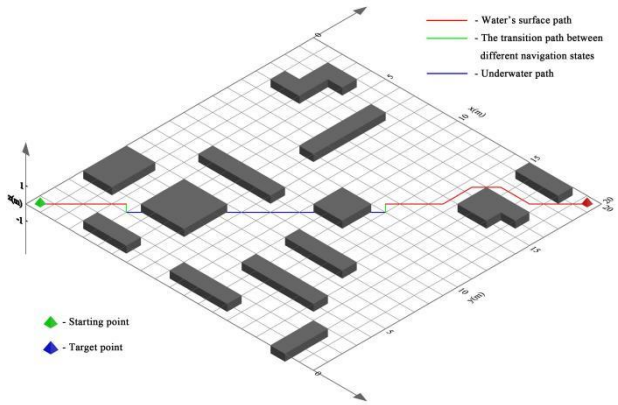

(a) The second type of path with a diving depth of 0.48m

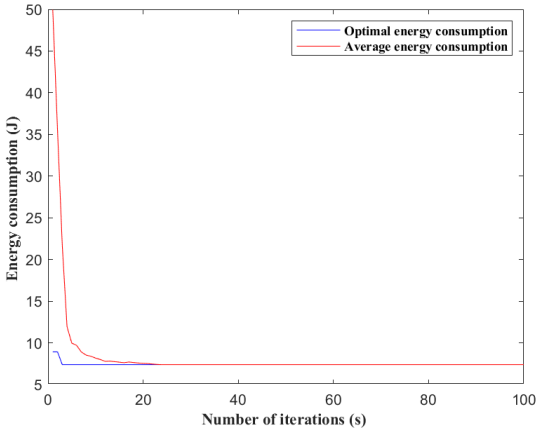

(b) Iterative diagram of water's surface path I

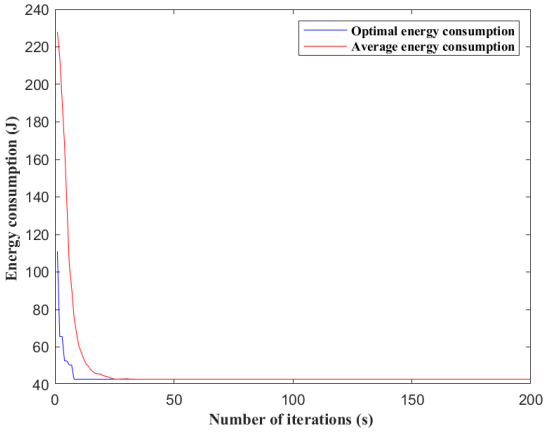

(c) Iteration diagram of underwater path

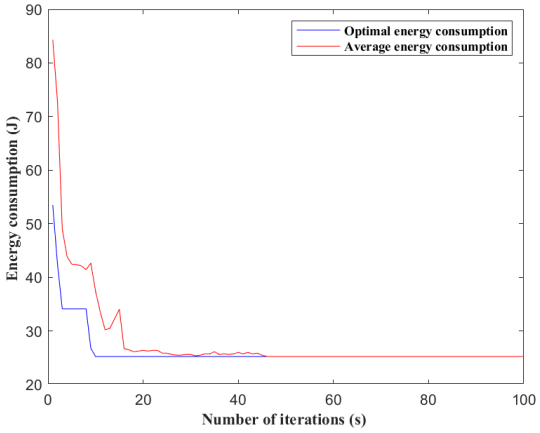

(d) Iterative diagram of water's surface Path Ⅱ

Figure 6. Path planning diagram and energy consumption iterative diagram for the second type of path within energy-saving-velocity in 3D navigation space (diving depth of 0.48m)

After completing the navigation task, the submersible unmanned ship has been navigating underwater at a determined depth until it passes all obstacles. The path graph and iterative graph of the second type of path are shown in Figure 7.

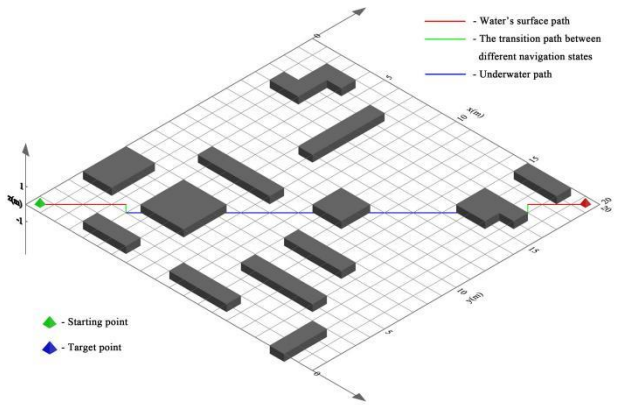

(a) The third type of path with a diving depth of 0.48m

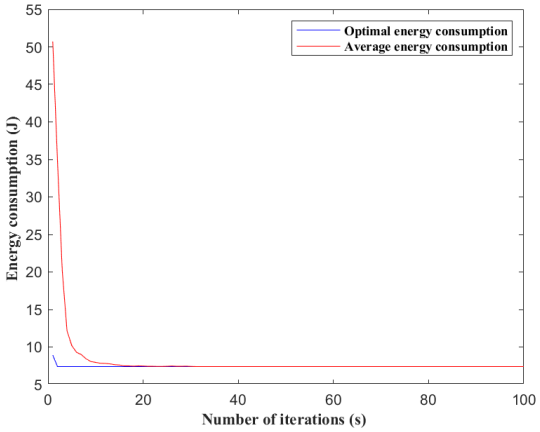

(b) Iterative diagram of water's surface path I

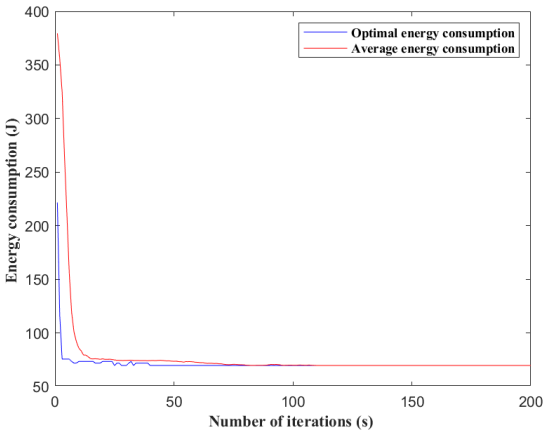

(c) Iteration diagram of underwater path

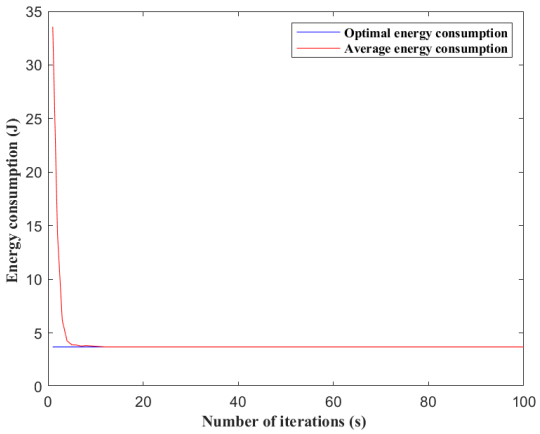

(d) Iterative diagram of water's surface Path Ⅱ

Figure 7. Path planning diagram and energy consumption iterative diagram for the third type of path witin energy-saving-velocity in 3D navigation space (diving depth of 0.48m)

When the energy-saving velocity is used, the simulation process and path types of the other three diving depths are the same as when the diving depth is 0.48m. The energy consumption values for the first type path of the submersible unmanned ship at four diving depths of 0.32m, 0.48m, 0.64m and 0.96m are 66.69J, 71.54J, 75.99J and 127.56J respectively. The energy consumption values of the second type of path at the above four dive depths are 67.28J, 78.31J, 88.15J and 213.80J, respectively. The energy consumption values for the third type of path are 66.33J, 83.55J, 98.78J and 298.51J, respectively.

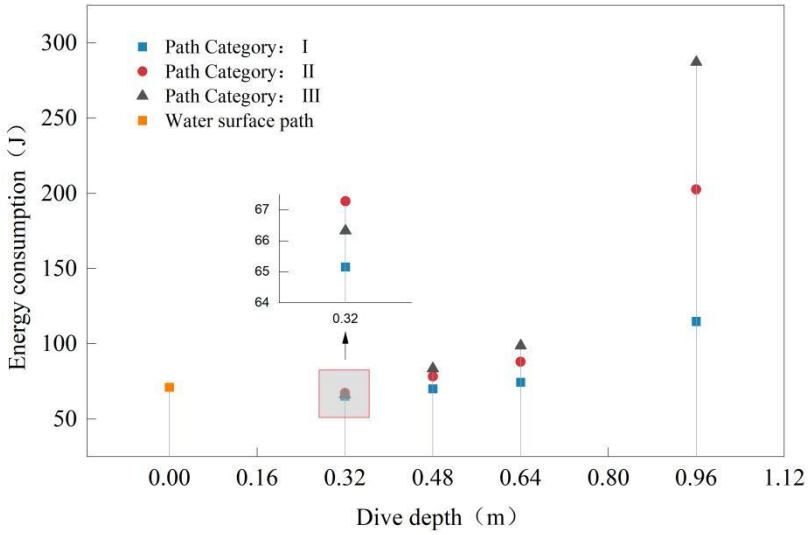

Figure 8. Diving depth – energy consumption diagram in 3D navigation space (energy-saving velocity)

The velocity of the submersible unmanned ship at different diving depths is the energy-saving velocity of each diving depth. With the increase of diving depth, the energy consumption values of the three types of navigation paths all showed an increasing trend.

(3) Comparison for single-navigation state and multy-navigation-states path simulation

At the energy-saving velocity, the energy consumption of the surface navigation path is greater than the energy consumption of three types of paths with a diving depth of 0.32m and less than that of the three types of paths with a diving depth of 0.96m. The energy consumption value of the surface navigation path is similar to that of a certain type of path for underwater diving with a depth of 0.48m or 0.64m.

5.3.2 Simulation of non-energy-saving-velocity path

The navigation area, path category and dive depth of the non-energy-saving-velocity path planning are the same as those of the energy-saving-velocity path planning. The only thing that has changed is the velocity of the submersible unmanned ship. The velocity is changed from the economic velocity of each diving depth to the non-energy-saving velocity, with the same velocity in all sailing states, and the path planning of the submersible unmanned ship at multiple non-energy-saving velocities is carried out. The velocity range is from 0.4m/s to 2m/s.

(1) Simulation analysis of single-navigation-state path for two-dimensional navigation space

In the two-dimensional navigation space, the non-energy-saving velocity surface path planning of the submersible unmanned ship is carried out. The path energy consumption at different velocities is shown in Figure 9.

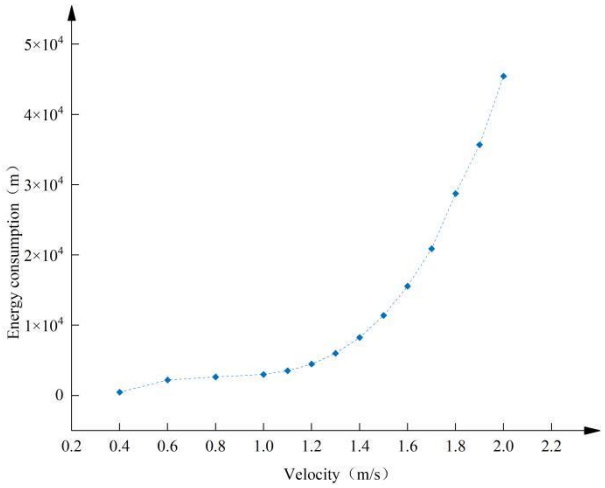

Figure 9. Two-dimensional navigation space velocity – energy consumption diagram (non-energy-saving velocity)

(2) Simulation analysis of multi-navigation-states path for three-dimensional navigation space

The process and method of non-energy-saving-velocity path planning in three-dimensional space is the same as that the energy-saving velocity path planning in three-dimensional space. After the diving depth is determined, the velocity of each sailing state in a complete path is the same. After the simulation, the path energy consumption value analysis of different velocities are carried out, and the entire velocity range is divided into three sections

The first velocity range is as follows: 0.4m/s–1.4m/s. Figure 10 shows the velocity-energy consumption diagrams of different depths in the velocity range.

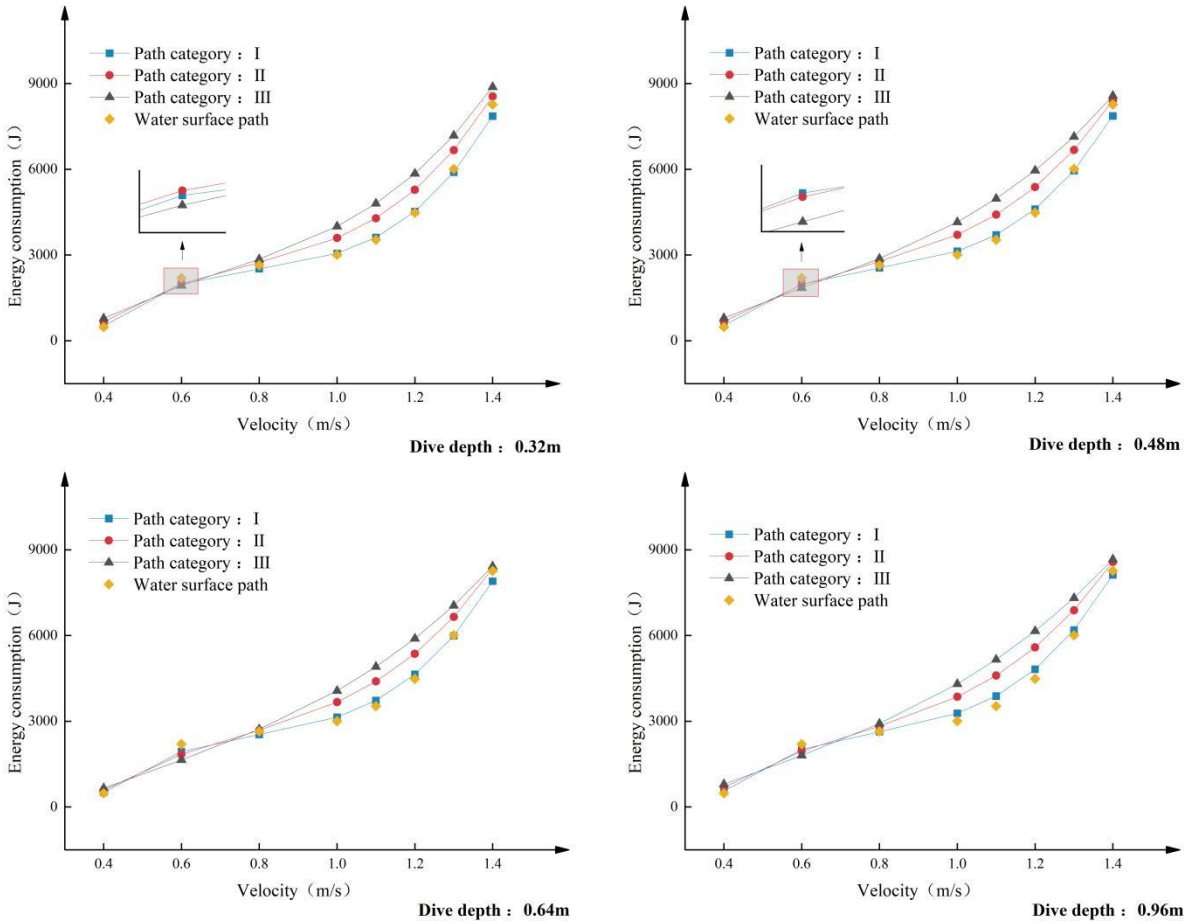

Figure 10. Velocity–Energy consumption diagram at different dive depths in 3D navigation space (velocity range: 0.4m/s–1.4m/s)

It can be seen from Figure 10 that:

①As the velocity increases, the energy consumption of each of the three types of navigation paths shows an upward trend.

②The sequence of energy consumption in three types of paths, under four dive depths within this velocity range except 0.6m/s, from high to low is: the energy consumption for the first type of path, the energy consumption for the second type of path, the energy consumption for the third type of path.

③The energy consumption of the surface navigation path of the submersible unmanned ship is mostly smaller than the energy consumption of the three types of navigation paths with navigation tasks.

The second velocity range is as follows: 1.4m/s–1.6m/s. Figure 11 shows the velocity-energy consumption diagrams of different depths in the velocity range.

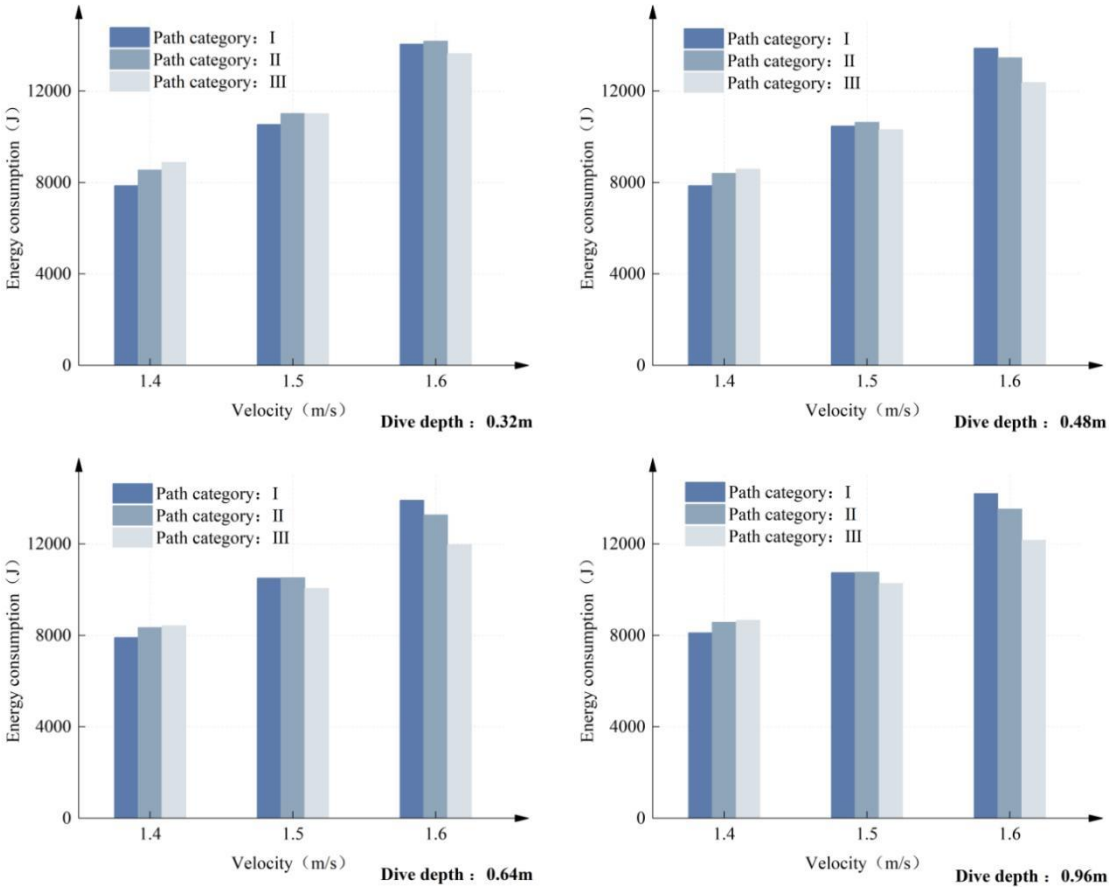

Figure 11. Velocity-energy consumption diagram at different depths in 3D navigation space (velocity range: 1.4m/s–1.6m/s)

It can be seen from Figure 11 that:

①At each determined diving depth, the energy consumption of each of the three types of navigation paths increases with the increase of the velocity.

②The variation law of the energy consumption of the navigation path of the submersible unmanned ship at the four diving depths is the same: the energy consumption of the first type of path changes from the lowest among the three types of paths, at 1.4m/s, to the highest or close to the highest, at 1.6m/s. The energy consumption of the third type of path changes from the highest, at 1.4m/s, to the lowest, at 1.6m/s.

The third velocity range was as follows: 1.6m/s–2m/s. Figure 12 shows the velocity-energy consumption diagrams of different depths in the velocity range.

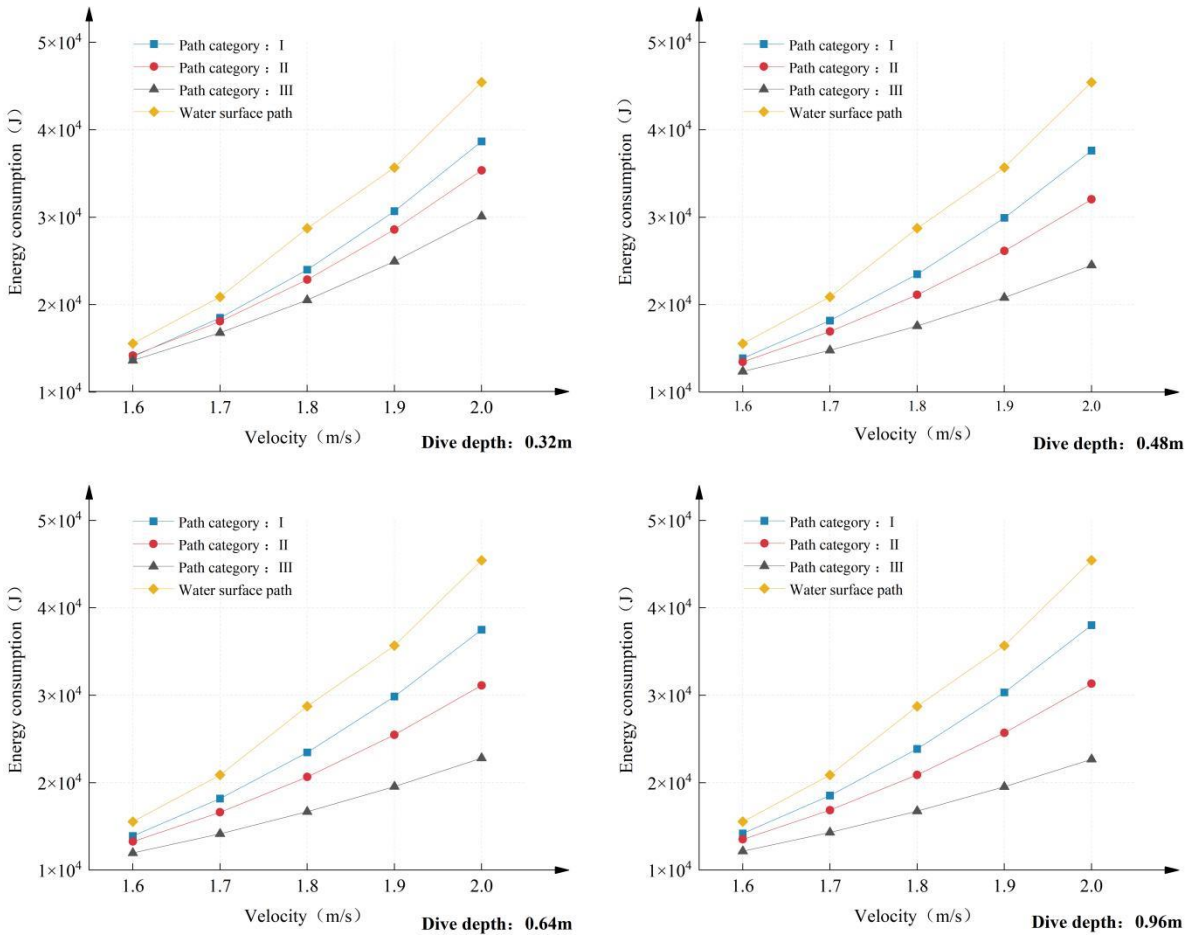

Figure 12. Velocity-energy consumption diagram at different depths in 3d navigation space (velocity range: 1.6m/s–2m/s)

It can be seen from Figure 12 that:

①As the velocity increases, the energy consumption of each of the three types of navigation paths still shows an upward trend.

②The sequence of energy consumption of the three types of paths, under the four diving depths within this velocity range, from high to low is: the energy consumption of the first type of path, the energy consumption of the second type of path, the energy consumption of the third type of path. The sequence of energy consumption for three types of paths within this velocity range is exactly opposite to that of the three types of paths in range of 0.4m/s~1.4m/s.

③The energy consumption of the surface navigation path of the submersible unmanned ship is greater than the energy consumption of the three types of paths with navigation tasks.

(3) Comparison for single-navigation-state and multi-navigation-states path simulation analysis

At the non-energy-saving velocity, before the velocity demarcation point 1.5m/s, the energy consumption of the three types of task-driven path are greater than that of water's surface path mostly. After the velocity demarcation point 1.5m/s, the energy consumption of the three types of task-driven paths are less than the energy consumption of water's surface path.

6 Conclusion and future work

(1) By applying the improved genetic algorithm, with the elite retention strategy and the adaptive adjustment function, the efficient optimisation of the path of the submersible unmanned ship, with the lowest energy consumption as the target, is realised.

(2) The velocity of the submersible unmanned ship is the energy-saving velocity, and the energy consumption value of the path increases with the increasing length of the underwater path when the diving depth is determined in a certain diving depth range

(0.32m, 0.48m, 0.64m, 0.96m). The energy consumption value of the same kind of path increases with increasing of the diving depth. When the speed of the diving unmanned ship is a non-energy-saving speed, the influence of the diving depth on the energy consumption of the navigation path is not obvious.

(3) The velocity of the submersible unmanned ship is a non-energy-saving velocity. When navigating in a two-dimensional navigation space, the energy consumption of the navigation path increases with increasing velocity within the velocity range of 0.4m/s–2m/s. The growth rate in the early stage is slow, and the growth rate in the later stage is faster.

(4)When the submersible unmanned ship sails in three-dimensional space at a non-energy-saving velocity, the energy consumption of the path still increases with increasing velocity. In addition, there is a velocity demarcation point in this non-energy-saving velocity range, and the sequence of energy consumption of the three types of paths before and after this point is reversed.

(5) When the submersible unmanned ship sails in three-dimensional space at a non-energy-saving velocity, the energy consumption changes without obvious rules when the diving depth is changed.

(6) The path energy consumption of the submersible unmanned ship depends on the sailing velocity, diving depth, route length of each sailing state, etc. The optimal navigation path needs to be determined according to the navigation task, the minimum diving depth and the navigation velocity.

In this paper, an improved genetic algorithm is used to optimise the path of the submersible unmanned ship, with the lowest energy consumption as the goal, and the corresponding conclusions are drawn after comparing the results under different navigation conditions. It provides certain technical support for path design research on cross-domain vehicles or unmanned ships. Nevertheless, there are still some limitations that must be further explored. First, the input parameters of the energy consumption model are affected by many factors. The real environment such as temperature, salinity wind, and waves will be considered and applied in the subsequent uncertainty analysis and hydrodynamic numerical simulation.Secondly, the current research is aimed at a specific submersible unmanned ship, and the adaptability of the established model to other ships or vehicles must be verified. Finally, the acceleration and deceleration process and navigation state transition process of the submersible unmanned ship in the actual path planning are the top priorities of the next research.

Acknowledgement

This work is supported by the National Natural Science Foundation of China (51879023) and the Central Government Guides Local Science and Technology Funds.

References

[1] Watkins, L.J., 2011. Self-propelled semi-submersibles: the next great threat to regional security and stability. Thesis Collection.

[2] Wang, W., 2016. The concept design and the analysis of the hydrodynamic performance of multi-navigation mode unmanned vehicle. (Doctoral dissertation, Harbin Engineering University).

[3] Liu, M.Y., Gao,L.T., Ma,X.Q., Peng, D.J., Wu, Y.L., 2021. Resistance analysis of multi-navigation mode new conceptual Ship. Ship engineering, 43(7), 7.

[4] Huo, C., Dong. Free running tests on navigation mode conversation of a latent high velocity craft. Journal of shanghai jiao tong university, 50(8), 6.

[5] Luo, F.Q., Huo, C., Gao, X,P., 2019. Experimental study on resistance of a multi-navigation mode high velocity unmanned craft. Ship science and technology, 41(23), 6.

[6] Algfoor, Z.A., Sunar, M.S., Abdullah, A., 2017. A new weighted path finding algorithms to reduce the search time on grid maps. Expert Systems with Applications, 71(APR.), 319-331.
[7] Eichhorn, M., 2017. Solutions for practice-oriented requirements for optimal path planning for the AUV "SLOCUM Glider". IEEE. IEEE.
[8] Hui, Y., Wang, Y., 2017. Multi-objective AUV Path Planning in Large Complex Battlefield Environments. Seventh International Symposium on Computational Intelligence & Design. IEEE.
[9] Gore, R., Pattanaik, K.K., Bharti, S., 2016. Dynamic path replanning algorithm for data gathering AUV. 2016 11th International Conference on Industrial and Information Systems (ICIIS). IEEE.
[10] Pan, X., Wu, X.S., Hou,X.G., Golble path planning based on genetic - ant hybrid algorithm for AUV. J. Huazhong Univ. of Sci. &. Tech. (Natural Science Edition),45(5), 6.
[11] Li, J., Zhang, R., Yu, Y., 2017. Multi-auv autonomous task planning based on the scroll time domain quantum bee colony optimization algorithm in uncertain environment. Plos One, 12(11), e0188291.
[12] Ramos, A.G., VJ García-Garrido., Mancho, A.M., Wiggins, S., Coca, J., Glenn, S., et al. 2018. Lagrangian coherent structure assisted path planning for transoceanic autonomous underwater vehicle missions. Scientific Reports, 8(1), 4575.
[13] Lin, Y.H., Huang, L.C., Chen, S.Y., Yu, C.M., 2018. The optimal route planning for inspection task of autonomous underwater vehicle composed of mopso-based dynamic routing algorithm in currents. Applied Ocean Research, 75, 178-192.
[14] Mahmoudzadeh, S., Powers, D., Sammut, K., Yazdani, A.M., Atyabi, A., 2018. Hybrid motion planning task allocation model for auv's safe maneuvering in a realistic ocean environment. Journal of Intelligent & Robotic Systems.
[15] Mahmoudzadeh, S., David, M., Sammut, K., Atyabi, A., Yazdani, A., 2018. A hierarchal planning framework for auv mission management in a spatio-temporal varying ocean. Computers & Electrical Engineering, 741-760.
[16] Sun, Y., Ran, X., Zhang, G., Xu, H., Wang, X., 2020. Auv 3d path planning based on the improved hierarchical deep q network. Journal of Marine Science and Engineering, 8(2), 145.
[17] Sayyaadi, H., Ura,T., Fujii,T., 2000. Collision avoidance controller for AUV systems using stochastic real value reinforcement learning method. Sice Sice Conference International Session Papers. IEEE.
[18] Sun, B., Zhu, D.Q., Tian, C., 2019. Complete coverage autonomous underwater vehicles path planning based on Glasius bio-inspired neural network algorithm for discrete and centralized programming [J]. IEEE transactions on cognitive and developmental systems, 11(1):73－84.
[19] Liu, G., Liu, P., Mu, W., & Wang, S., 2016. A path optimization algorithm for auv using an improved ant colony algorithm with optimal energy consumption. Hsi-An Chiao Tung Ta Hsueh/Journal of Xi'an Jiaotong University, 50(10), 93-98.
[20] Alvarez, A., Caiti, A., & Onken, R., 2004. Evolutionary path planning for autonomous underwater vehicles in a variable ocean. IEEE Journal of Oceanic Engineering, 29(2), 418-429.
[21] Witt, J., & Dunbabin, M., 2008. Go with the flow: Optimal AUV path planning in coastal environments. In Australian conference on robotics and automation (Vol. 2008, No. 2).
[22] Miao, R.L.,2013. Path planning of Energy-Conservation for autonomous underwater vehicle. (Doctoral dissertation, Harbin Engineering University).
[23] Zhang, C., Zhang, D., Zhang, M., & Mao, W., 2019. Data-driven ship energy efficiency analysis and optimization model for route planning in ice-covered Arctic waters. Ocean Engineering, 186, 106071.